Cu segregation in Au–Cu nanoparticles exposed to hydrogen atmospheric pressure: how is fcc symmetry maintained?

Q. Wang, A. Nassereddine, D. Loffreda, C. Ricolleau, D. Alloyeau, C. Louis, L. Delannoy, J. Nelayah, H. Guesmi

Cu segregation in Au-Cu nanoparticles exposed to hydrogen atmospheric pressure: how is fcc symmetry maintained?

Q. Wang[1], A. Nassereddine[2], D. Loffreda[3], C. Ricolleau[2], D. Alloyeau[2], C. Louis[4], L. Delannoy[4], J. Nelayah[2*], H. Guesmi[1*]

1 ICGM, Univ. Montpellier, CNRS, ENSCM, Montpellier, France

2 Université Paris Cité, CNRS, Laboratoire Matériaux et Phénomènes Quantiques, 75013 Paris, France

3 ENSL, CNRS, Laboratoire de Chimie UMR 5182, 46 Allée d'Italie, 69364 Lyon, France

4 Sorbonne Université, CNRS, Laboratoire de Réactivité de Surface, LRS, Paris, France

** jaysen.nelayah@u-paris.fr ; hazar.guesmi@umontpellier.fr*

ABSTRACT

In a recent, work [Nassereddine et al. Small 2021, 2104571] we reported the atomic-scale structure and dynamics of sub-4nm sized Au nanoparticles (NPs) supported in titania in H_2 at atmospheric pressure obtained by using aberration-corrected environmental transmission electron microscopy (ETEM), density functional theory (DFT) optimizations and *ab initio* molecular dynamic (AIMD) simulations. Our results showed unstable Au NPs losing their initial face-centred cubic (*fcc*) symmetry (from *fcc* to non-*fcc* symmetries) and revealed the drastic effect of hydrogen adsorption. In this work, we use the same approach to study the dynamics of equiatomic Au-Cu NPs in the same range of size and the results show an enhanced structural stability upon alloying by Cu. In spite of the morphology evolution from facetted to rounded shapes, the observed Au-Cu NPs are found to keep their *fcc* symmetry under atmospheric hydrogen pressure. AIMD simulation evidences Cu segregation process from the sub-surface toward the upper surface layer, and a reversed segregation of Au atoms from the surface

towards the sub-surface sites. The analysis of the chemical ordering in the core shows a tendency to a local chemical ordering where Au-Cu hetero-atomic bindings are favoured. The segregating Cu seems to play a major role in reducing the fluxionality of Au-Cu NPs in H_2 and thus, maintaining their *fcc* symmetry.

1. INTRODUCTION

Small sized nanoparticles (NPs) have been attracting growing interest in heterogeneous catalysis due to their large surface-to-volume ratio, which makes them very active [1]. However, their small size induces problems of stability in the harsh chemical environment where these nanoparticles operate [2-3]. Moreover, responsive structural transformations may occur and cause catalyst deactivation, especially under high-temperature reaction conditions [4]. Generally, the stabilization of small metallic NPs can be achieved through either chemical interactions between the metal species and the support or alloying [5, 6]. Indeed, by choosing a suitable promoter that can generate synergetic effects, the NPs can be strongly stabilized from catalytic point of view [7]. In addition, in many cases, the use of bimetallic alloys is shown to increase the catalytic performances (better activity and/or selectivity and better stability of the activity with time on stream) of catalyst NPs.

The first major advance in bimetallic catalysts was occurred in 1968 with the addition of Re to promote Pt catalysts [8]. These bimetallic catalysts were shown to be more stable than the monometallic Pt, allowing work at lower pressures, which increases the selectivity to aromatics. A very large number of studies have since focused on bimetallic catalysts, for a wide range of applications [9-12]. Among them, the Au-Cu combination has been the subject of a large number of works because of the very high miscibility of these two metals [13-17]. Moreover, the Au-Cu catalysts were found to be more active, stable and selective than their monometallic counterparts in a number of catalytic reactions [17-20]. A structural evolution of the alloyed bimetallic Au-Cu nanoparticles during the reaction was reported in some cases, especially under

O_2 atmosphere and during CO oxidation, resulting in Au–CuO core/shell structure [21-25]. In hydrogenation reactions, such structural modifications have not been experimentally evidenced yet, but it was tentatively proposed that the initial increase in activity observed for Au-Cu/TiO_2 catalysts during butadiene hydrogenation was related to copper segregation, induced by the reactants, at the surface of the bimetallic nanoparticles [26]. Similarly, several studies in the literature have shown that the structure of the Au-Cu NPs and the ability of Au and Cu to form an alloy have a crucial influence on their activity [27-28]. However, as far as we know, there are no studies in the literature allowing confirming or refuting the hydrogen induced segregation and/or alloying processes in Au-Cu nanoalloys and a clear picture at the atomic level of the structure and the chemical ordering in presence of adsorbates is still missing. This is critical for a fundamental understanding of their stability and their intrinsic catalytic properties.

In a very recent work [29], combined *in situ* ETEM observations under hydrogen at atmospheric pressure and varied temperature, and ab initio molecular dynamic (AIMD) simulations showed that monometallic Au NPs of sub-4nm size lose their initial *fcc* symmetry (*fcc* symmetry under vacuum *vs* non-*fcc* or icosahedral symmetries under hydrogen) and are highly fluctuating. In contrast, no changes were observed on bigger sized Au NPs (> 4 nm). The strong structural instability of small sized Au NPs was shown to result from the strong motion of atoms from the center toward the sub-surface layers and *vice-versa*, induced by the hydrogenated gold surface and the formed H-Au-H-Au crowned lines surrounding the distorted core [29]. In this work, we show that alloying Au by Cu induces stabilization of the NPs and prevents the structural fluctuations under atmospheric hydrogen pressure exposure as the case of monometallic Au counterpart. Indeed, *in situ* ETEM observations show sub-4nm equiatomic Au-Cu NPs maintaining their initial *fcc* structure under H_2. For temperatures between 400 and 200 °C, they undergo a modification of their morphology, but hydrogen interaction does not induce any modification of their crystalline structure. In order to gain atomic scale insights into the structural

dynamics and the atomic ordering of Au-Cu NPs exposed to hydrogen and to compare with our previous results on pure Au NPs, DFT calculations (at 0K) and AIMD simulations at 227°C (500K) were performed on model truncated octahedral hydrogen-covered Au and Au-Cu NPs of 201-atoms. The energetic stability of different configurations of Au_{101}-Cu_{100} covered by 1ML of atomic hydrogen was calculated and the structure evolution dynamics of the optimal configuration was followed. Surface Cu enrichment and local ordering tendency of the core are predicted under hydrogen.

2. EXPERIMENTAL AND THEORETICAL DETAILS

Sample preparation: Gold-copper nanoparticles supported on TiO_2 (100% anatase, US research nanomaterials, surface area 50 $m^2.g^{-1}$, purity = 99.98%) were synthesized by deposition-precipitation with urea method, as described in detail in [30-31]. Here, we targeted NPs with an equiatomic composition ($Au_{50}Cu_{50}$) and a metal loading of 3 wt% and 1 wt% for Au and Cu, respectively. In order to reach the targeted metal composition and metal loading, 2 g of TiO_2 support and the appropriate amount of the two metal precursors $Cu(NO_3)_2.3H_2O$ (Sigma-Aldrich) and $HAuCl_4.3H_2O$ (Sigma-Aldrich) were first mixed in a double-wall reactor followed by the addition of an excess of urea $CO(NH_2)_2$ ([urea]/ [metal] = 100) to the solution. The mixture was then stirred for 20 h at 80 °C in the dark to avoid uncontrolled reduction of the gold precursor. The solid obtained was separated from the liquid solution by centrifugation. After centrifugation, the solid was washed three times with distilled water in order to eliminate impurities and especially chlorine residues (chlorides). The sample was further dried under vacuum at room temperature for 24 h, and then activated by heat treatment at 300 °C under H_2 at atmospheric pressure to reduce the metal precursors into metal nanoparticles. For *in situ* electron microscopy studies in gas environments, the sample was transferred to air after the heat treatment under H_2 and deposited in a dedicated gas nanoreactor.

In situ environmental TEM: In situ environmental TEM observations of TiO_2 supported gold-copper NPs supported on TiO_2 were carried out in double aberration-corrected JEOL ARM 200F microscope. The microscope was equipped with a cold field emission gun operating at 200 kV in the present work. For the observation the Au-Cu NPs in gas phase, at high temperature and pressure conditions, we used a Protochips Atmosphere TEM environmental high-pressure gas cell (HPGC). The HPGC consisted of two silicon microchips called E-chips. The small E-chip (2 mm × 2 mm × 300 µm) was designed with a 50 nm thick electron-transparent SiN window at its center. As for the large E-chip (6 mm × 4.5 mm × 300 µm), it was patterned with six 30 nm thick electron-transparent SiN windows. The two E-chips were aligned and assembled in closed-cell configuration at the tip of a dedicated TEM sample holder in such a way that the two sets of SiN windows were aligned. For ETEM observations, the Au-Cu NPs were deposited on the large E-chip by drop casting 6 µl of a suspension of Au-Cu/TiO_2 sample ultrasonically dispersed in distilled water. The NPs were subjected to pure argon (Messer, purity > 99.999%) and pure hydrogen (Messer, purity > 99.999%) under static gas conditions. The sample was heated through resistive heating on the large E-chip. *In situ* observations of Au-Cu NPs were performed in STEM mode, using both HAADF and BF detectors. For image acquisition, we employed an electron beam with a diameter of about 0.8 Å and a probe current of 27 pA. The convergence semi-angle was set to 20.5 mrad and the inner and outer collection semi-angles was equal to 68 and 280 mrad, respectively for HAADF imaging. In BF mode, the collection semi-angle was limited to 17 mrad. High-resolution STEM images (2048 × 2048 pixels) were acquired at ×10M magnification with pixel area equal to 8.97×10^{-3} $Å^2$. To limit radiation damage during in situ STEM imaging, all images were captured with a limited time frame rate of 2 or 3 µs per pixel. Moreover, the electron illumination was blanked between image acquisition. The dose per frame, as defined in [32], was around 5×10^4 $e^- Å^{-2}$.

Cluster models: Pure (TOh_Au_{201}) and bimetallic (TOh_Au_{101}-Cu_{100}) regular truncated octahedron NP models of 1.8 nm size (201 atoms) were considered to represent the observed

ETEM NPs. The bimetallic TOh_$Au_{101}Cu_{100}$ NPs were of equi-atomic composition with 101 and100 Au and Cu atoms, respectively. The NP models had an fcc symmetry and were formed by a core of 13 atoms, an inner-shell (also named subsurface in the text) of 66 atoms and an outer-shell (the surface) of 122 atoms. To represent a maximum of possible alloy types, seven NP configurations with different Au and Cu chemical ordering were constructed (see Figure 1) by either substituting 100 Au atoms and replacing them by Cu in a DFT optimized TOh_Au_{201} NP or by substituting 4 Au atoms and replacing them by Cu in an ordered L_{10} phase TOh_Au_{105}-Cu_{96}. This latter ordered structure was found to be stable either for the case of large sized Au-Cu [33] and Au-Pd [34] NPs.

- Configuration 1 (conf_1): the Au atoms occupied all bulk sites (13 atoms in the core + 66 atoms in the inner-shell) and some surface edge sites (22 atoms). All Cu atoms were on the NP surface.
- Configuration 2 (conf_2): A Janus-like structure was constituted by Au atoms on one side and Cu atoms on the other side.
- Configuration 3 (conf_3): The initial structure was the L_{10} –ordered phase where Cu enriched the core.
- Configuration 4 (conf_4): 13 Au atoms constituted the core. The Cu atoms occupied the 66 inner-shell sites and 4 (111) facets (22 surface sites). The remaining Au atoms occupied the surface sites.
- Configuration 5 (conf_5): The Cu atoms occupied all bulk sites (13 atoms in the core + 66 atoms in the inner-shell) and some surface facet sites (22 atoms) forming Cu dimers. All Au atoms were on the surface.
- Configuration 6 (conf_6): The initial structure was the L_{10} –ordered phase where Au enriched the core.
- Configuration 7 (conf_7): 13 Au atoms composed the core, 66 Cu atoms composed the inner-shell and the outer-shell was formed by hetero atomic phase where the remaining

Cu atoms were surrounded by Au atoms, and occupied the (111) and (100) surface facet sites.

-

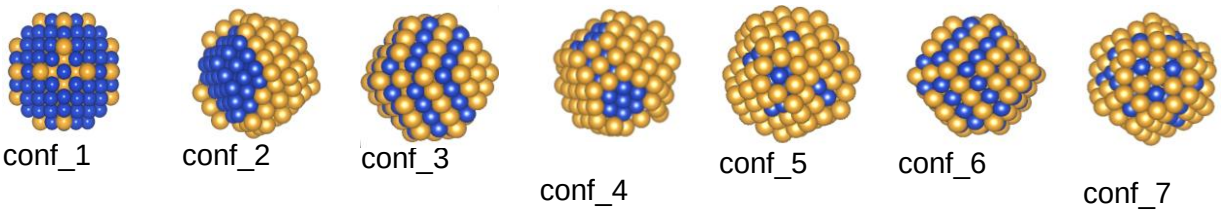

Figure 1: The seven constructed configurations of TOh_$Au_{101}Cu_{100}$. Blue and yellow balls correspond to Cu and Au atoms, respectively.

In order to take into account the presence at the atmospheric hydrogen pressure, 122 H atoms were adsorbed on the facets of the Au (TOh_$Au_{201}H_{122}$) and Au-Cu (TOh_$Au_{101}Cu_{100}$, from conf_1 to conf_7) NPs, which corresponds to a 1ML hydrogen coverage. The considered 1ML hydrogen coverage consists of H atoms mainly occupying two-fold bridge and three-fold hollow sites. Modeling Au-Cu NPs in absence and in presence of hydrogen was performed using a cubic cell of dimensions

DFT calculations and AIMD simulations: DFT calculations and *Ab-Initio* Molecular Dynamics simulations were performed using Vienna *ab initio* Simulation Package (VASP 5.4.1) [35-36]. The Generalized Gradient Approximation functional of the exchange–correlation energy was calculated within the Perdew, Burke, and Ernzerhof formulation of the generalized-gradient approximation (GGA-PBE) [37-38]. Dispersion corrected PBE-D3 functional proposed by Grimme [39] were included to account for Van der Waals interactions. The cut off energy was fixed to 400 eV. Fine geometry optimizations were performed by choosing a convergence threshold of 10^{-6} eV for the total electronic energy and a threshold of $\pm 10^{-2}$ eV·Å^{-1} for minimizing residual forces acting on the nuclei. The interactions of hydrogen with the metallic NPs were

quantified by calculating the adsorption energy normalized by the number of H atoms (N_H_{ads}) (eq.1):

$\Delta Eads = [E(TOh+adsorbate) – E(TOh) – E(adsorbate)]/N\_H_{ads}$, eq1.

where E(TOh+adsorbate), E(TOh), E(adsorbate) were the calculated electronic energy of H species adsorbed on metallic NPs, of bare TOh NPs ((Au NPs and Au-Cu NPs from conf_1 to conf_7), of gas phase H_2, respectively. The adsorption energy per H atom refered to $1/2H_2$ (g).

Ab Initio Molecular Dynamics simulations involving Born-Oppenheimer approximation were performed in the canonical (NVT) ensemble employing Nosé-Hoover thermostat [40-41] with a time step of 1fs at 500K with a total integration time of 20 ps. The NP models used for AIMD simulations (TOh_Au_{101}-Cu_{100}-H_{122}) were initially optimized by DFT. Then, local minimum energy structures associated with specific atomic arrangements selected from MD simulations were isolated and their geometrical and electronic properties recalculated and analyzed by DFT method. Let us note, that as reported in our previous study [29], since the shape of the observed NPs immediately changed upon H_2 exposure, we supposed that H_2 readily dissociates over the surface of Au and Au-Cu NPs resulting in adsorbed atomic hydrogen.

3. RESULTS AND DISCUSSION

Experimental observations:

The structural dynamics of a 2.3 nm Au-Cu NP supported on TiO_2 under static H_2 at atmospheric pressure as a function of temperature was followed *in situ* by STEM high angle annular dark field (HAADF) and bright field (BF) imaging (Figure 2.A and B). In addition, Figure 2.C shows the Fast Fourier transform (FFT) of the high resolution BF STEM images. This particle size belongs to the critical size domain (≤ 4 nm) showing strong structural instability under H_2 for monometallic Au NPs [29]. As a reference, the NP was initially imaged under residual Ar gas at 400 °C showing a facetted particle (see evidenced facets in Figures S1) with *fcc* symmetry structure (Figure 2.A-C

a) which is the well known symmetry bulk Au-Cu alloys under vacuum [42]. 10^5 Pa H_2 was then introduced, and the sample was cooled in 100 °C steps from 400 to 200 °C. At each temperature step, the structural parameters of the NP were followed as a function of time. As temperature is lowered, a continuous evolution of the morphology of the nanoparticle toward the rounded shape is observed as a result of its interaction with H_2 molecules (the 2D projection of the nanoparticle shows that the morphology remains rounded on average) (Figure 2.A,B b-e). However, unlike Au NPs of the same size range [29], the Au-Cu NP retains its *fcc* crystalline structure even under prolonged exposure to H_2 (up to around 2 hours at 200 °C). Indeed, indexing of the FFT of the STEM BF images (Figure 2.C) shows the resolution of the (111) lattice planes of the fcc structure.

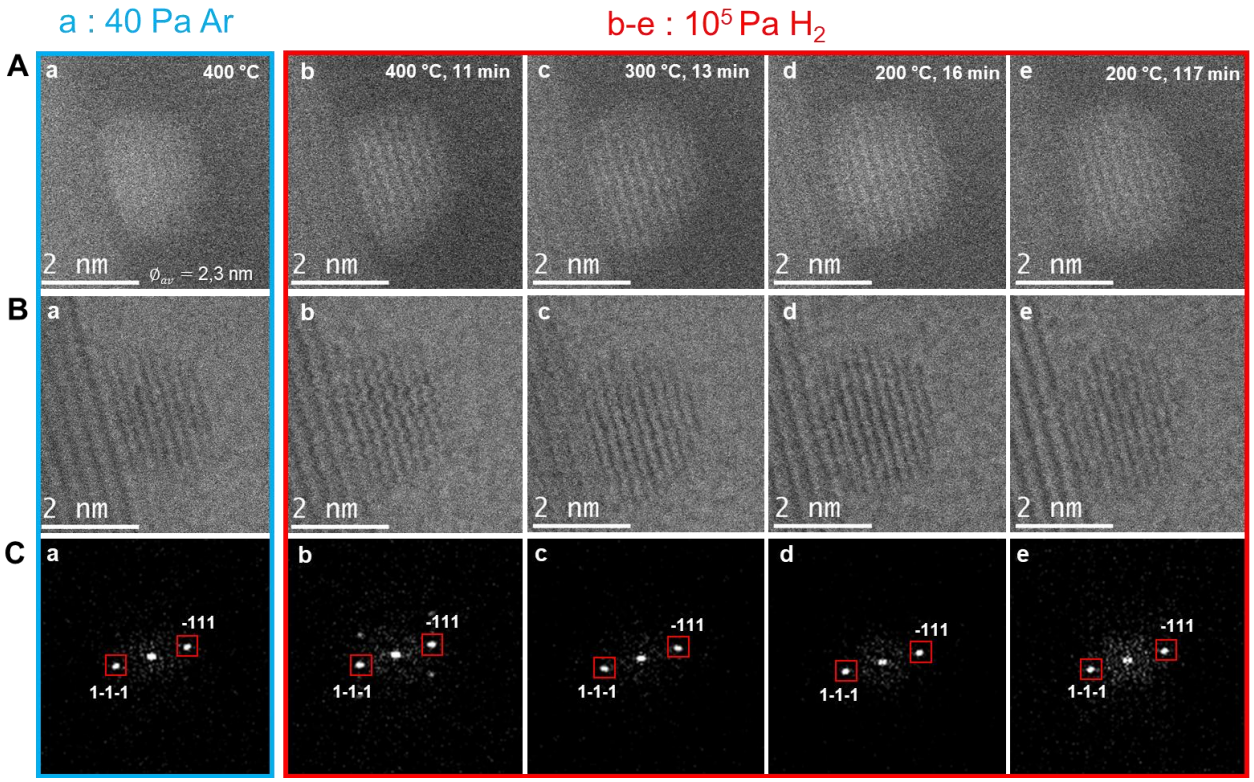

Figure 2: Atomic scale visualization of the structural stability of a Au-Cu NP of a size of 2.3 nm supported on anatase TiO_2 support in H_2 at atmospheric pressure. (A-B) STEM HAADF (A a-e)

and BF (B a-e) STEM images of the NP acquired *in situ* at (a) 400 °C under 40 Pa Ar, (b) 400 (c) 300 and (d,e) 200 °C under 10^5 Pa H_2 , showing a continuous evolution of the morphology of Au-Cu NP under H_2 but with no change in crystal structure. (C) FFT of the high resolution BF STEM images showing a stable *fcc* nanoparticle structure between 400 and 200 °C.

Theoretical calculations:

In order to understand how the Au-Cu NPs retain their fcc symmetry while the Au ones lose them under H_2, DFT geometry optimizations were firstly performed on TOh Au and TOh_Au-Cu model NPs of 201 atoms covered by 1ML of atomic hydrogen. Then AIMD simulations at 500 K were run to follow the trajectory of a selected hydrogenated Au-Cu NP during a simulation time span of 20 ps. Upstream work consisted of checking the effect of temperature by performing AIMD simulation at 500K for bare TOh_Au_{201}. The results of radial distribution and the probability distribution functions of Au relative to the center of mass reported in the supplementary information (Figure S2) show no effect of the applied temperature on neither on the shape nor on the fcc symmetry of Au NP.

DFT optimizations of Au-Cu NP configurations*:* The different considered Au-Cu model NPs from conf_1 to conf_7 were optimized under vacuum and in presence of hydrogen. The Figure 3 shows the energetic stability diagram of the different isomers (described in Section 2) where the upper side of the figure indicates the results obtained under vacuum and the lower part those obtained for different isomers in presence of 1ML adsorbed atomic hydrogen.

Under vacuum, the relative stabilities of isomers are calculated by taking the most stable configuration (conf_7) as the reference. The energetic phase diagram shows that the optimum structures are those with the surface enriched by Au atoms. Conf_1 where all Cu atoms are in the surface outer shell and all Au atoms in the bulk (the inner_shell and the core) is found to be highly unfavorable (+26.7 eV). The results are consistent with the fact that the lower surface energy and larger size of Au compared to Cu, induce better stability of Au on the NP surface

sites. The Janus-like structure (conf_2) is also found to be unfavorable by more than +7.5 eV, which agrees with the tendency of Au-Cu bulk alloy to form ordered phases instead of separated phases. Furthermore, conf_3 and conf_6 having L10 like-ordered phase structures are found to be endothermic by 4.5 eV and 3.7 eV, respectively, with a better stability for conf_6 which includes a pure Au core of 13 atoms. The lower stability of ordered phase Au-Cu in our model NPs is in line with the results of J-Q. Goh et al [33] who showed that phase ordered minima are always unfavorable for NPs of 201 atoms. The Au rich core is also found to characterize the most stable structure conf_7, for which the inner-shell is completely composed by Cu atoms and the remaining Cu atoms are located on the surface the terrace sites of the (111) facets and are surrounded by Au surface neighbors. Subsurface position of Cu atoms may help in decreasing the atomic pressure [33, 16, 43] while alternating Au-Cu surface, Cu inner shell and Au core may increase the chemical ordering.

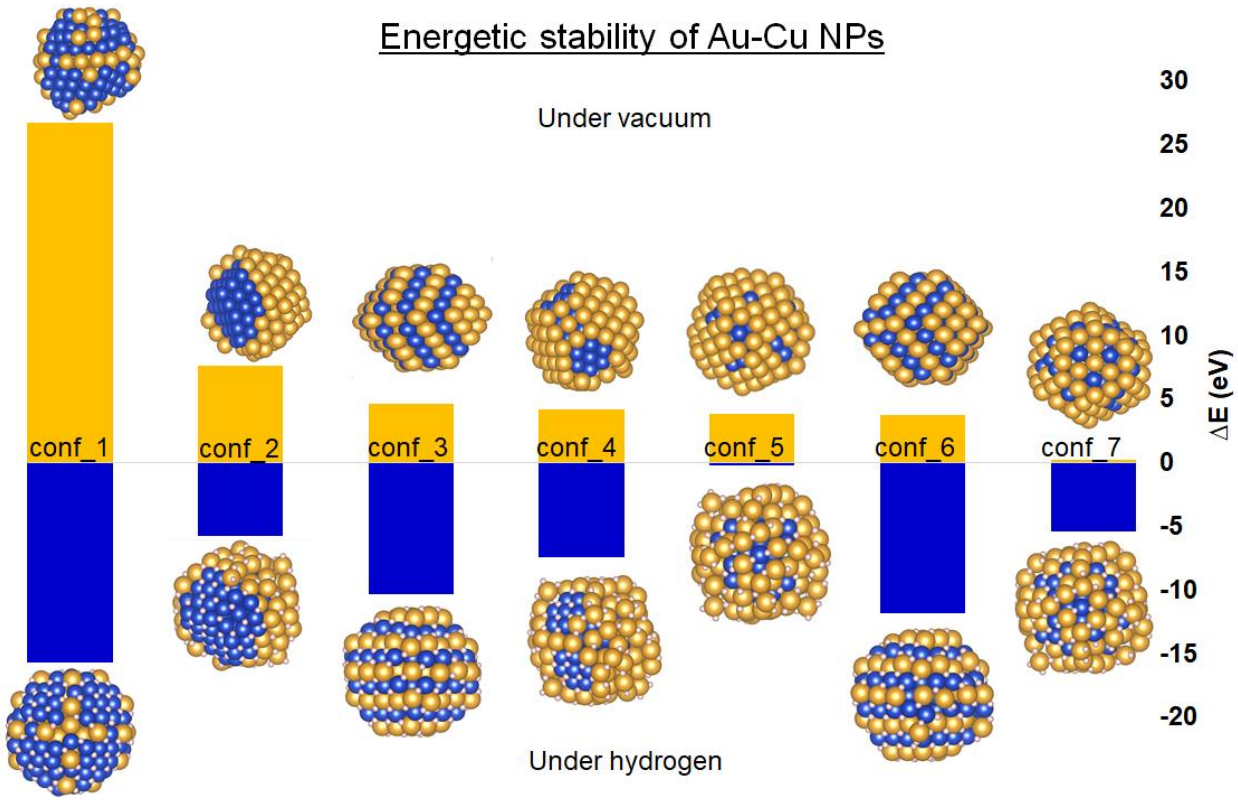

Figure 3.: Energetic stability of computed TOh_$Au_{101}Cu_{100}$ isomers under vacuum and in

presence of presence of 1ML of adsorbed atomic hydrogen. Zero energy reference is taken as the highest total energy structure for under vacuum case (conf_7) and as the lowest total energy configuration in hydrogen (conf_5). Blue and yellow balls correspond to Cu and Au atoms, respectively. Small white balls represent the adsorbed hydrogen atoms.

Considering the hydrogen covered NPs, the relative stabilities of isomers were calculated by taking as a reference the lowest stable configuration (conf_5). As depicted in Figure 3, the conf_5 where all Au atoms are located on the surface is now the least stable configuration. In contrast, the conf_1 where all the Cu atoms are located in the surface and in direct interaction with adsorbed hydrogen, is found to be the most stable stable (-15.7 eV). This result indicates a strong tendency of Cu to segregate toward the surface, which agrees with its higher affinity with hydrogen than Au. Moreover, the adsorption energy of hydrogen on the conf_1 is found to be exothermic by -0.21 eV/H compared to pure Au NP (+0.08 eV/H) while it is found to be endothermic for all other Au-Cu isomers (see Table S1). Let us note that the adsorption energies of atomic hydrogen (referenced with respect to H2 in gas phase) are calculated for 1ML coverage where repulsive interaction between H adsorbates is high. In addition, these energetic values represent an average adsorption energy of hydrogen on different surface adsorption sites and the adsorption of H atoms on sites as corners and edges may be more exothermic. These latter under-coordinated surface sites were reported to be dissociative sites of H_2 molecules in several experimental and theoretical works [44-47]

The relative energetic stabilities of ordered phase configurations conf_6 and conf_3 are calculated to be of -11.9 eV and -10.4 eV, respectively, in favor of the configuration with Au rich core (conf_6). Finally, the conf_7, which is predicted to be the most stable configuration under vacuum, is less stable than the conf_4 while their main difference is the position of surface Cu

atoms, showing by the way a tendency of surface Cu atoms to form Cu-Cu bonds in presence of adsorbed H atoms.

AIMD simulations at 500K in presence of hydrogen:

The predicted DFT minimum energy configurations of H covered Au and Au-Cu NPs (conf_7) were considered as the initial configurations for AIMD simulations. Figure 4 shows the minimum energy structures of Au and Au-Cu NPs extracted from AIMD trajectories at t=0 and t=20 ps where the shape of both NPs is found to change from TOh to rounded one, in agreement with the ETEM observations. Upon few ps of simulation time at 500K, Au located on the edge sites readily form H-Au-H-Au chains with hydrogen atoms located in bridge sites. For the case of pure Au NP, the length of these chains grow continuously assembling up to few dozen of connected H and Au atoms [for more details see 29]. Considering the Au-Cu NP, local phenomenon of Cu segregation from the sub_surface towards the surface and Au surface diffusion toward the subsurface layer are observed during the time simulation of 20 ps (video S1). The number of Cu surface atoms interacting with hydrogen increases from 22 atoms at t=0 ps to about 48 atoms at t=18 ps, which is about half of the total number of Cu atoms of the NP. This Cu surface enrichment induces the progressive breaking of H-Au-H-Au chains interspersed by segregated Cu atoms. Interestingly, the surface Cu atoms are also found to diffuse on the surface and to form H-Cu-H-Cu chains of few atoms long (up to 4 Cu atoms during 20 ps of time simulation, see video S2) that grow with time. The analysis of atomic structure of the formed chains shows Au-Au bond length in the range of [2.72 Å -2.83Å] and shorter Cu-Cu bond lengh in the range of [2.59 Å -2.39 Å].

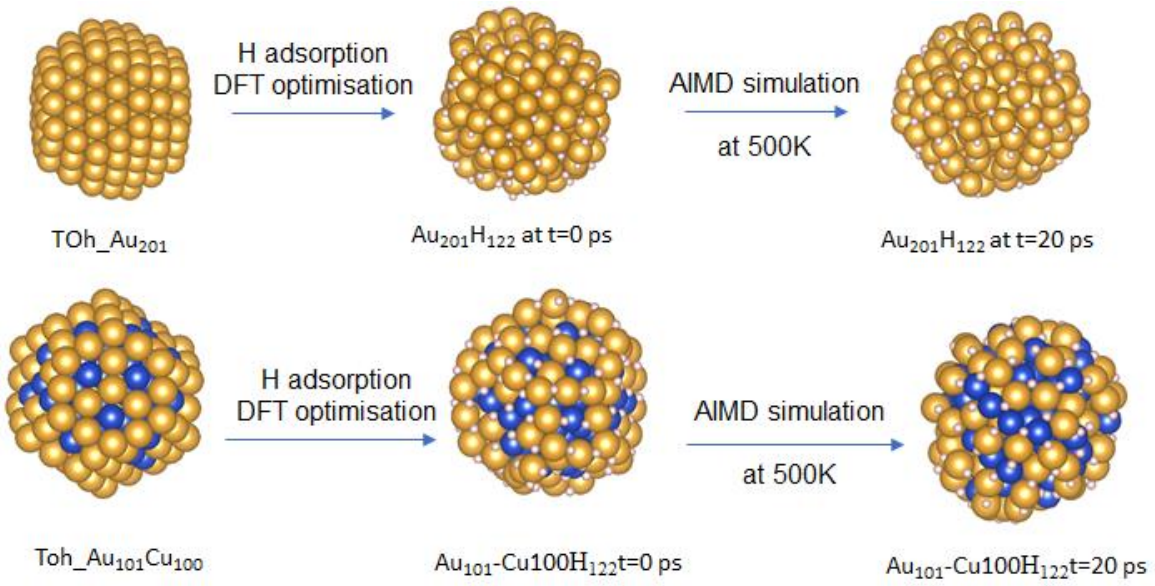

Figure 4.: Evolution of the shape and surface structure of Au and Au-Cu (conf_7) NPs after the adsorption of hydrogen atoms from DFT optimization and AIMD simulation. Blue, yellow and small white balls represent Cu, Au and H, respectively.

The analysis of the atomic evolution of the bimetallic NP core also reveals some surprising behavior. Indeed, several Cu atoms are found to segregate from the subsurface towards the pure Au core and *vice-versa* indicating a tendency of the hydrogenated Au-Cu NP to form chemically ordered core structure. To elucidate this behavior, the initially optimized H covered Au-Cu configurations conf_1 and conf_7 were re-optimized by substituting the central Au atom in the core by a Cu atom. The substituted Au atom was then, placed on the surface. Unexpectedly, both configurations were found to stabilize by up to 0.3 eV and 0.6 eV, respectively. This result indicates the tendency of Au-Cu core to form hetero-atomic Au-Cu bindings.

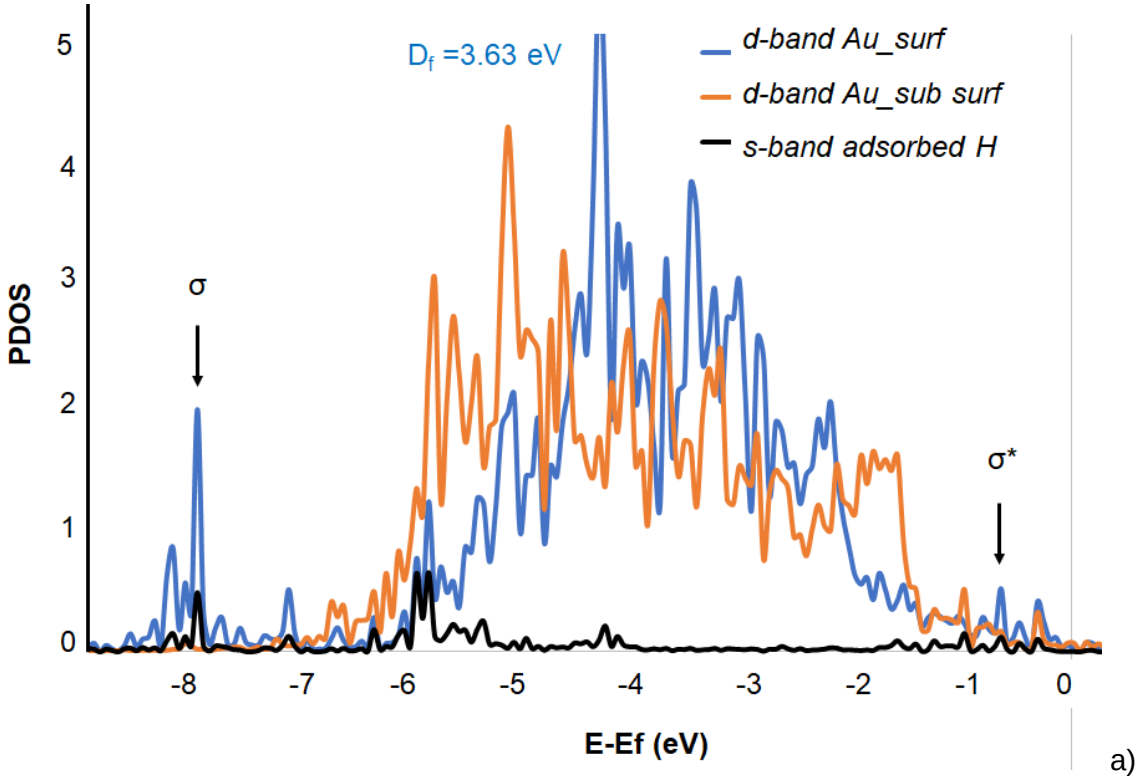

a)

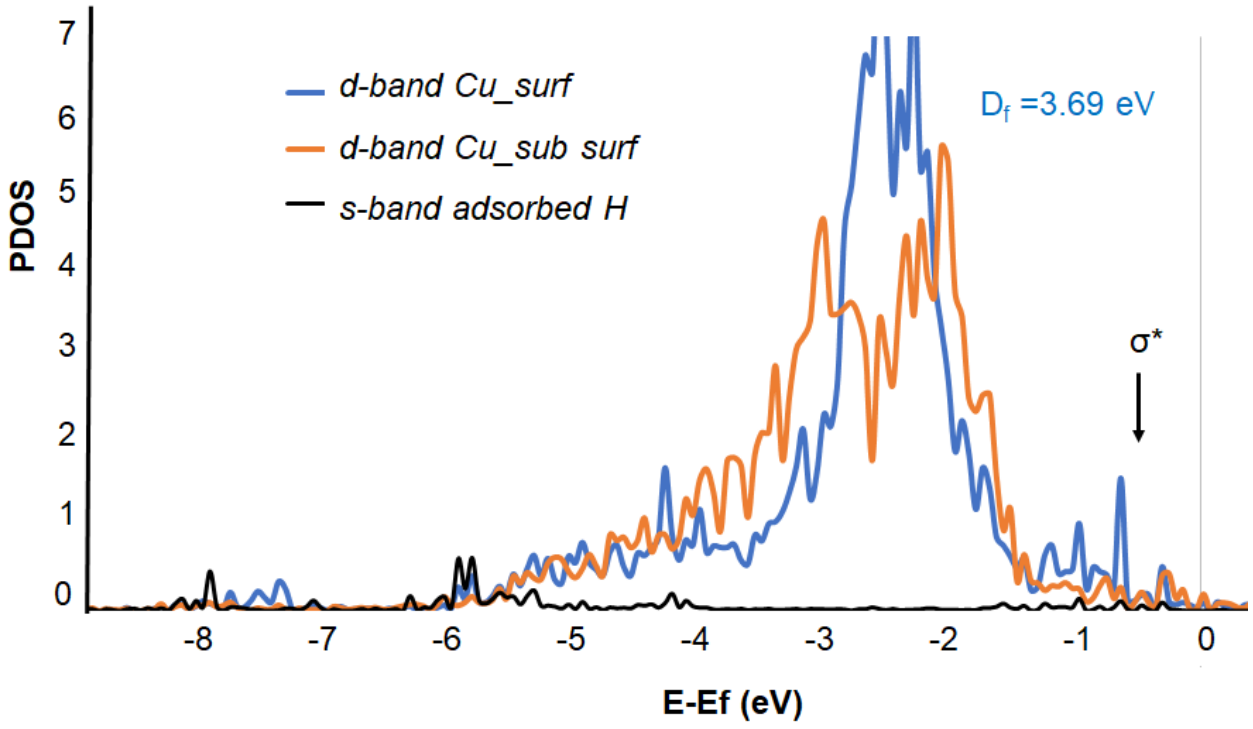

b)

Figure 5: Electronic structure analyses of the optimized DFT structures of hydrogenated Au-Cu

NP extracted after time simulation of 16 ps. (a) Au 5d-band density of states of Au on the surface (direct interaction with H) and with neighboring Au located in the subsurface. The d-band centers of Au surface and subsurface atoms are calculated to be of -3.63 eV and -3.69 eV, respectively. (b) 4d-band density of states of Cu on the surface (direct interaction with H) and with neighboring Cu located in the subsurface. The d-band centers of Cu and subsurface Cu atoms are calculated to be of -2.59 eV and -2.68 eV, respectively. The s orbital of the hydrogen atom interacting with Au and Cu is also reported.

Further analyses were performed to determine how strongly the interaction with hydrogen affects the electronic structure of Au-Cu NP. Minimum energy configuration extracted from the AIMD trajectories of hydrogenated Au-Cu conf_7 was quenched at 0 K and its geometry was optimized by DFT. The computed total energy indicates better stability by more than +0.5 eV with respect to the hydrogenated Au-Cu conf_1. In Figure 5 are reported the calculated distribution of the projected (local) density of states (PDOS) of Au and Cu atoms from the surface (i.e. interacting with hydrogen in bridge sites) and those of neighboring Au and Cu atoms from the subsurface. For Au surface atoms, the PDOS distribution shows sharp peaks around -8 eV which correspond to the interaction of hydrogen (σ bonding state) with the s (not presented here) and the d bands of Au, both of which undergoing significant changes. These peaks are not observed in the case of Cu surface atoms. Close to the Fermi level, even smaller in the value, anti-bonding states, σ*, are observed in the d-zone of copper and gold surface atoms and the s orbital of the hydrogen atom. The relatively pronounced anti-bonding states observed for copper surface atom compared to Au may learn about the stronger adsorption of hydrogen on Cu inducing its surface segregation. As reported by L. Yu et al. [48], the electrons that would occupy the high-energy anti-bonding states are transferred to the Fermi-level, leading to an energy gain that may largely control surface bonding. Concerning the subsurface atoms, changes in the distribution of the local density of states for Au and Cu atoms are found to be much smaller, which contrasts with

the large spatial perturbation region not only limited to the upper surface layer. Interestingly, the comparison of the calculated *d*-band centers of the density of states of Au and Cu from the surface and from the subsurface show a shift from the Fermi level towards the negative values in the case of subsurface atoms (from 3.63 eV to -3.69 eV for Au and from -2.59 eV to -2.68 eV for Cu). This result may indicate a charge transfer processes from the hydrogenated surface atoms to subsurface atoms, predicted to be stronger in the case of Cu. For pure hydrogenated gold NP [29], the charge transfer was found to take place from the core toward the surface, which revealed a complex and non-intuitive behavior. In summary, if the chemical properties of our small sized Au and Au-Cu NPs, could be determined, to a certain degree, by the local density of d-states lying below the Fermi level, further analysis of the sp-states, which are smaller in value but near the Fermi level, as well as the anti-bonding electron transfers [48] using more accurate level of theory, would be useful. This will be the subject of a near-future work.

CONCLUSION

Fifteen years ago, in the Faraday Discussion 138, G. Bond reported in his concluding remarks the following sentence:" Failure to consider why a particular structure or composition behaved as it did, betrays a lamentable lack of curiosity, and retards the development of basic theory". In this work, we have endeavoured to go further than a "simple report" of the observed structural dynamics of Au-Cu small NPs under gas and we tried to provide an atomistic picture of the evolving nanoalloy system and its related electronic properties. First, it should be recalled how it is challenging to observe by ETEM such a small sized bimetallic NPs (smaller than 4 nm) under H_2 atmospheric pressure. These microscopy observations provide valuable characterisations of the NPs evolutions that may occur during the catalytic processes, as for example during hydrogenation reactions. In this work, we showed using ETEM that while the morphology of Au-Cu NPs evolves under H_2 at atmospheric pressure, their *fcc* symmetry was maintained. These

observations differ from those of Au NPs in the same range of size, which loses their *fcc* symmetry upon the interaction with hydrogen. Indeed, while hydrogen is known to weakly interact with Au, it is found to induce drastic changes of both the surface and the core structures leading to a change of the symmetry of the whole particle [29]. In contrast, at first stage, hydrogen seems to affect only the surface atoms in the case of Au-Cu NPs. DFT calculations and AIMD simulation bring some insights to the processes happening during hydrogen exposure and reveal the segregation of Cu atoms from the subsurface towards the surface sites. The evolving surface seems to organize in the form of linear chains of H-Cu-H-Cu with hydrogen in bridge sites separated by H-Au-H-Au chains encircling the core, which may explain the rounded particle shape observed experimentally. Atomic scale analysis of the Au-Cu NP core structure evidences a tendency towards a local chemical ordered whereby Au atoms tend to be surrounded by Cu ones (also diffusing from the subsurface). If one could extrapolate the atomic reorganisation after long time equilibration (unfortunately unreachable by calculations), the structure of Au-Cu NPs might evolve towards structures with a Au-Cu core with local chemical order and a surface and a subsurface enriched in Cu. The chemical ordering tendency of the core may be at the origin of the reduction of the fluxionality of Au atoms and the maintenance of the fcc symmetry in Au-Cu NPs, inducing by the way their better stabilisation compared to pure Au NPs.

SUPPORTING INFORMATION

Supporting Information is available free of charge on the RCS publication website or from the author.

ACKNOWLEGEMENTS

This work was supported by the French National Research Agency through the TOTEM project, Grant Number ANR-17- CE07-0031. A. N was supported by a PhD fellowship granted through

the same project. The authors are grateful to Region Ile de France for convention SESAME E1845 for the support of the JEOL electron microscope installed at Université de Paris. The authors thank IDRIS in Paris, CINES in Montpellier, TGCC in Grenoble (project 609 and A0090807369, GENCI/CT8) and especially PSMN in Lyon for CPU time and assistance. The authors thank the CPER/SYSPROD 2015-2022 project (N°2019-AURA-P5B) and AXELERA Pôle de Compétitivité (PSMN Data Center). The authors are also grateful to GDR Or-Nano (GDR n°2002) for his work to stimulate effective collaborations. H. G.is grateful to C. Mottet for faithful discussions and for providing L10 ordered phase structure of model NPs derivated from SMA calculations.

Author Informations

These authors contribute equally: Qing Wang, Abdallah Nassereddine

J. N, H. G conceived the ideas. A.N, L.D and C.L fabricated the samples. A.N and J.N performed the electron microscopy experiments and analysed the TEM data with D.A and C.R. A.N. and J.N carried out the STEM simulations. Q.W, H.G and D.L carried out the numerical simulations. All authors contributed to the preparation of the paper. H.G and J.N supervised the project.

REFERENCES

1 M. Che and C. O. Bennett, *The Influence of Particle Size on the Catalytic Properties of Supported Metals*, Elsevier, 1989.

2 L. Xu, H. W. Liang, Y. Yang and S. H. Yu, *Chem. Rev.,* 2018, **118**, 3209.

3 R. Narayanan and M. A. El-Sayed, *J. Am. Chem. Soc.,* 2003, **125**, 8340.

4 L. C. Liu and A. Corma, *Trends in Chemistry,* 2020, **2**, 383.

5 J. Wisniewska, H. Guesmi, M. Ziolek and F. Tielens, *J. Alloys Compd.,* 2019, **770**, 934.

6 R. Ferrando, J. Jellinek and R. L. Johnston, *Chem. Rev.,* 2008, **108**, 845.

7 H. T. Phan and A. J. Haes, *J. Phys. Chem. C Nanomater Interfaces,* 2019, **123**, 16495.

8 H. E. Kluksdahl, *Reforming a Sulfur-Free Naphtha with a Platinum-Rhenium Catalyst*, US Patent, 1968.

9 J. H. Sinfelt, *Bimetallic catalysts: Discoveries, concepts, and applications*, Wiley-Interscience, 1983.

10 F. F. Tao, *Chem. Soc. Rev.* 2012, **41**, 7977.

11 O. G. Ellert, M. V. Tsodikov, S. A. Nikolaev and V. M. Novotortsev, *Russian Chemical Reviews,* 2014, **83**, 718.

12 H. Guesmi. Gold Bullt. 2013, 46 (4) 213-219.

13 Han, Y. L. Wang, T. Z. Ma, W. Li, J. L. Zhang, M. H. Zhang, *Front. Chem. Sci. Eng.,* 2020, **14**, 689.

14 G. Rossi, R. Ferrando, A. Rapallo, A. Fortunelli, B. C. Curley, L. D. Lloyd, R. L. Johnston, *J. Chem. Phys.,* 2005, **122**, 194309.

15 R. Ferrando, A. Fortunelli and R. L. Johnston, *Phys. Chem. Chem. Phys.,* 2008, **10**, 640.

16 M. Dhifallah, M. Iachella, A. Dhouib, F. Di Renzo, D. Loffreda and H. Guesmi, *J. Phys. Chem. C,* 2019, **123**, 4892.

17 C. L. Bracey, P. R. Ellis and G. J. Hutchings, *Chem. Soc. Rev.,* 2009, **38**, 2231

18 A. Sandoval, C. Louis and R. Zanella, *Appl. Catal. B,* 2013, **140**, 363.

19 P. Mierczynski, K. Vasilev, A. Mierczynska, W. Maniukiewicz, M. I. Szynkowska and T. P. Maniecki, *Appl. Catal. B,* 2016, **185**, 281.

20 D. Kim, J. Resasco, Y. Yu, A. M. Asiri and P. Yang, *Nat. Commun.,* 2014, **5**, 4948.

21 X. Y. Liu, A. Q. Wang, L. Li, T. Zhang, C. Y. Mou and J. F. Lee, *J. Catal.,* 2011, **278**, 288.

22 E. Volker, F. J. Williams, E. J. Calvo, T. Jacob and D. J. Schiffrin, *Phys. Chem. Chem. Phys.,* 2012, **14**, 7448.

23 A. Wilson, A. Bailly, R. Bernard, Y. Borensztein, A. Coati, B. Croset, H. Cruguel, A. Naitabdi, M. Silly, M. C. Saint-Lager, A. Vlad, N. Witkowski, Y. Garreau and G. Prevot, *Nanoscale,* 2019, **11**, 752.

24 X. Guo, X.-Q. Sun, Y. Guo, Y.-L. Guo, Y.-S. Wang, L. Wang and W.-C. Zhan, *Rare Metals,* 2021, **40**, 1056.

25 S. Zafeiratos, S. Piccinin and D. Teschner, *Catal. Sci. Technol.,* 2012, **2**, 1787.

26 L. Delannoy, G. Thrimurthulu, P. S. Reddy, C. Methivier, J. Nelayah, B. M. Reddy, C. Ricolleau and C. Louis, *Phys. Chem. Chem. Phys.,* 2014, **16**, 26514.

27 J. C. Bauer, D. Mullins, M. Li, Z. Wu, E. A. Payzant, S. H. Overbury and S. Dai, *Phys. Chem. Chem. Phys.,* 2011, **13**, 2571.

28 X. Liu, A. Wang, X. Wang, C. Y. Mou and T. Zhang, *Chem Commun (Camb),* 2008, 3187.

29 A. Nassereddine, Q. Wang, D. Loffreda, C. Ricolleau, D. Alloyeau, C. Louis, L. Delannoy, J. Nelayah and H. Guesmi, *Small,* 2021, **17**, e2104571.

30 R. Zanella, S. Giorgio, C. R. Henry and C. Louis, *J. Phys. Chem. B,* 2002, **106**, 7634.

31 R. Zanella, L. Delannoy and C. Louis, *Appl. Catal. A: Gen.,* 2005, **291**, 62.

32 P. Abellan, T. J. Woehl, L. R. Parent, N. D. Browning, J. E. Evans and I. Arslan, *Chem Commun (Camb),* 2014, **50**, 4873.

33 J. Q. Goh, J. Akola and R. Ferrando, *J. Phys. Chem. C,* 2017, **121**, 10809.

34 B. E. Zhu, A. Front, H. Guesmi, J. Creuze, B. Legrand and C. Mottet, *Comput. Theor. Chem.,* 2017, **1107**, 49.

35 G. Kresse and J. Hafner, *Phys. Rev. B Condens. Matter,* 1993, **47**, 558.

36 G. Kresse and J. Furthmuller, *Phys. Rev. B Condens. Matter,* 1996, **54**, 11169.

37 J. P. Perdew, K. Burke and M. Ernzerhof, *Phys. Rev. Lett.,* 1996, **77**, 3865.

38 J. P. Perdew, J. A. Chevary, S. H. Vosko, K. A. Jackson, M. R. Pederson, D. J. Singh and C. Fiolhais, *Phys. Rev. B Condens. Matter,* 1992, **46**, 6671.

39 S. Grimme, J. Antony, S. Ehrlich and H. Krieg, *J. Chem. Phys.,* 2010, **132**, 154104.

40 W. G. Hoover, *Phys. Rev. A: Gen. Phys.,* 1985, **31**, 1695.

41 S. Nosé, *J. Chem. Phys.,* 1984, **81**, 511.

42 H. Okamoto, D.J. Chakrabarti, D.E Laughlin, and T.B. Massalski,1987, **8**(5), 454.

43 M. Dhifallah, A. Dhouib, S. Aldulaijan, D. I. R. F and H. Guesmi, *J. Chem. Phys.,* 2016, **145**, 024701.

44. E. Bus, J. T. Miller, J. A van Bokhoven, Hydrogen chemisorption on Al2O3-supported gold catalysts. The Journal of Physical Chemistry B 2005, 109(30), 14581-14587.

45. M. Boronat, P. Concepción, A. Corma, Unravelling the nature of gold surface sites by combining IR spectroscopy and DFT calculations. Implications in catalysis. The Journal of Physical Chemistry C 2009, 113(38), 16772-16784.

46. A. C. Gluhoi, H. S.Vreeburg, J. W. Bakker, B. E. Nieuwenhuys, Activation of CO, O2 and H2 on gold-based catalysts. Applied Catalysis A: General 2005, 291(1-2), 145-150.

47.L. Álvarez-Falcón, F. Viñes, A. Notario-Estévez, F. Illas, On the hydrogen adsorption and dissociation on Cu surfaces and nanorows. Surf. Sci. 2016, 646, 221-229.

48 L. Yu, Q. Yan, A. Ruzsinszky, *Phys. Rev. Mat.* 2019, **3**, 092801(R)